Electronic Supplementary Material (ESI) for Journal of Materials Chemistry C.

Supplementary Information

Reactive spin coating based on real-time In-Situ feedback for improved control of perovskite thin film fabrication

Simon Biberger[1], Maximilian Spies[1], Konstantin Schötz[1], Frank-Julian Kahle[1], Nico Leupold[2], Ralf Moos[2], Helen Grüninger[3], Anna Köhler[1], Fabian Panzer[1#]

[1]Soft Matter Optoelectronics (EP II), University of Bayreuth, Bayreuth 95440, Germany

[2]Department of Functional Materials, University of Bayreuth, Bayreuth 95440, Germany

[3]Northern Bavarian NMR Centre (NBNC) and Inorganic Chemistry, University of Bayreuth, Bayreuth 95440, Germany

Corresponding Author:

[#]E-Mail: fabian.panzer@uni-bayreuth.de

Section 1: In-Situ Spin coater Setup and fitting details

Figure S1: Photographs of the optical in situ spin coater setup used for the reactive spin coating approach, together with the connected syringe pump used for the antisolvent dispensing.

The setup for measuring the in situ optical data during spin-coating is shown in figure S1. It consists of a custom-built spin-coater with a hole in the middle. Underneath the spin-coater a white-light LED is placed. Its light shines through the hole in the middle of the spin coater and serves as a white light source for transmission measurements. A laser diode (405 nm) in combination with focusing optics and a diaphragm are mounted above the spin-coater for exciting the sample for PL measurements. The circular area probed by our optical measurements during the spin coating has a diameter of 5 mm in the center of the substrate. White-light and excitation laser are turned on and off alternatingly, so that either transmission or PL is probed. Transmitted light and PL are collected with one optical fiber, which is coupled to the detection system. The detection system consists of a CCD camera, coupled to a spectrograph, and a home-built detection setup, which is described in detail in Supporting Reference 1.[1] In brief, the detection setup switches the optical path between transmission and PL

measurements, so that for PL measurements, the laser wavelength is blocked by a suitable filter. In contrast, for transmission measurements, the transmitted light is coupled into the spectrograph without additional filtering. The detection setup further synchronizes the CCD camera with the white-light LED, the laser and the optical path switching. Using this setup, we can record PL and transmission during spin-coating quasi-simultaneously (i.e., alternating frame by frame) with a rate of 15 Hz. From the transmission measurements, the optical density (OD) is calculated based on a reference measurement prior to spin-coating. The antisolvent is automatically dispensed via a syringe pump (Model 540060, TSE Systems) through a connected capillary and pipette tip.

Derivation of eq. (2)

Given the following relation:

$$d = \frac{\lambda_1 \lambda_2}{2(\lambda_1 n_2 - \lambda_2 n_1)} \tag{S1}$$

where d is the thickness of the film, λ_1 and λ_2 are the wavelengths of two consecutive extrema in the OD. n_1 and n_2 are the refractive indices of the sample at the respective wavelengths. Assuming that n is constant in the investigated spectral range and is given by the refractive index of dimethylformamide (n_{DMF}) yields:

$$d = \frac{\lambda_1 \lambda_2}{2(\lambda_1 - \lambda_2) n_{DMF}} \tag{S2}$$

The frequency ω of the observed sine wave in units of energy is given by

$$\omega = \frac{2\pi}{E_2 - E_1} \tag{S3}$$

where E_1 and E_2 are the energetic positions of two consecutive extrema in the OD. Using the Planck constant h and speed of light c, one is able to rewrite the energy in terms of wavelength:

$$\omega = \frac{2\pi}{\frac{hc}{\lambda_2} - \frac{hc}{\lambda_1}} = \frac{2\pi}{hc} \frac{\lambda_1 \lambda_2}{\frac{\lambda_1 \lambda_2}{\lambda_2} - \frac{\lambda_1 \lambda_2}{\lambda_1}} = \frac{2\pi}{hc} \frac{\lambda_1 \lambda_2}{\lambda_1 - \lambda_2} \tag{S4}$$

Inserting eq. (S4) into eq. (S2) yields:

$$d = \frac{hc\omega}{4\pi\, n_{DMF}} \tag{S5}$$

Section 2: $MAPbI_3$

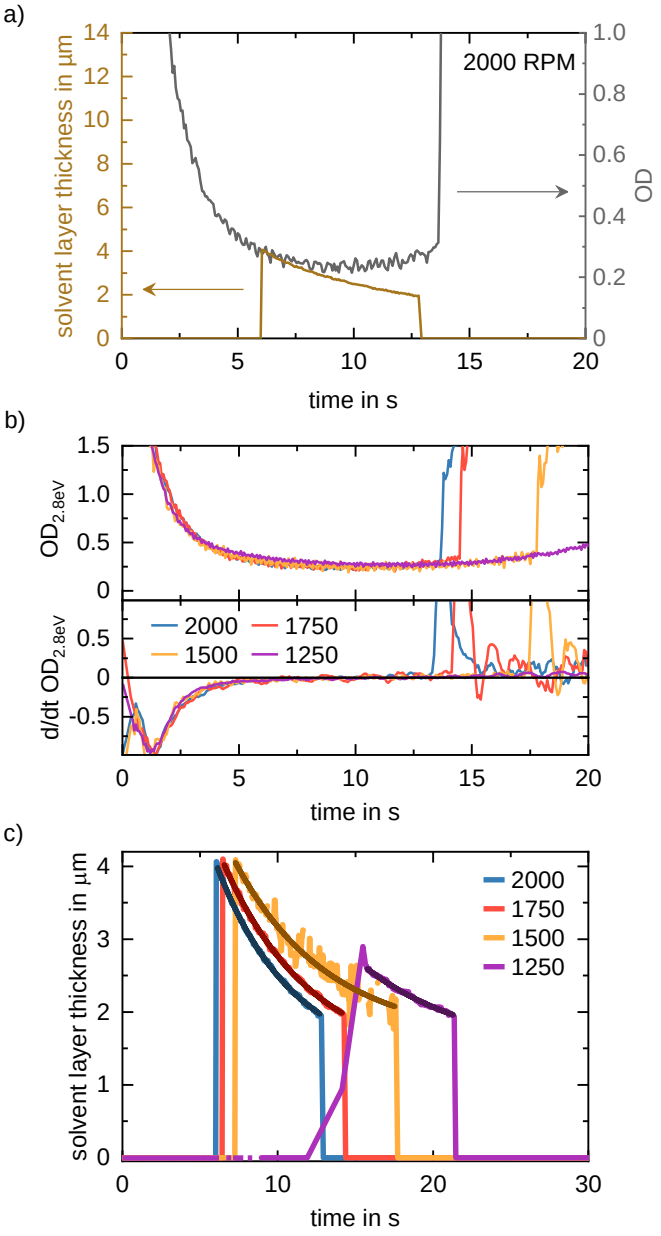

Figure S2: a) Evolution of the solvent layer thickness (ocher), together with the evolution of the OD at 2.8 eV (grey) for the film spin coated at 2000 RPM. b) Evolution of the OD at 2.8 eV for all four spin speeds (top) and the respective first time-derivatives (bottom) c) Evolution of the solvent layer thickness for all four spin speeds.

At the beginning of the observable interference pattern, both the solution layer thickness and the OD at 2.8 eV follow the same qualitative decrease. While the solution layer thickness continuously keeps decreasing, the OD at 2.8 eV stays constant after

5 s (see d/dt $OD_{2.8\ eV}$ in Figure S2b). The fast decrease of the OD at the start indicates a throw-off of precursor solution. Afterwards the OD stays constant and only the solvent layer thickness decreases. This suggests a mere evaporation of the solvent. Since the exact description of the thinning of film during spin coating is complex,[2] we determined a rate constant as a measure for the thinning process of the solvent films due to evaporation for the different spin speeds by fitting the evolution of the solvent layer thickness with a mono-exponential decay. The resulting rate constants for all spin speed are summarized in table S1.

Table S1: Evaporation rate constants extracted from mono-exponential fitting of the evolution of the solvent layer thickness for all spin speeds.

Spin speed in RPM	2000	1750	1500	1250
rate constant in 1/s	0.205 ± 0.003	0.176 ± 0.003	0.169 ± 0.014	0.147 ± 0.011

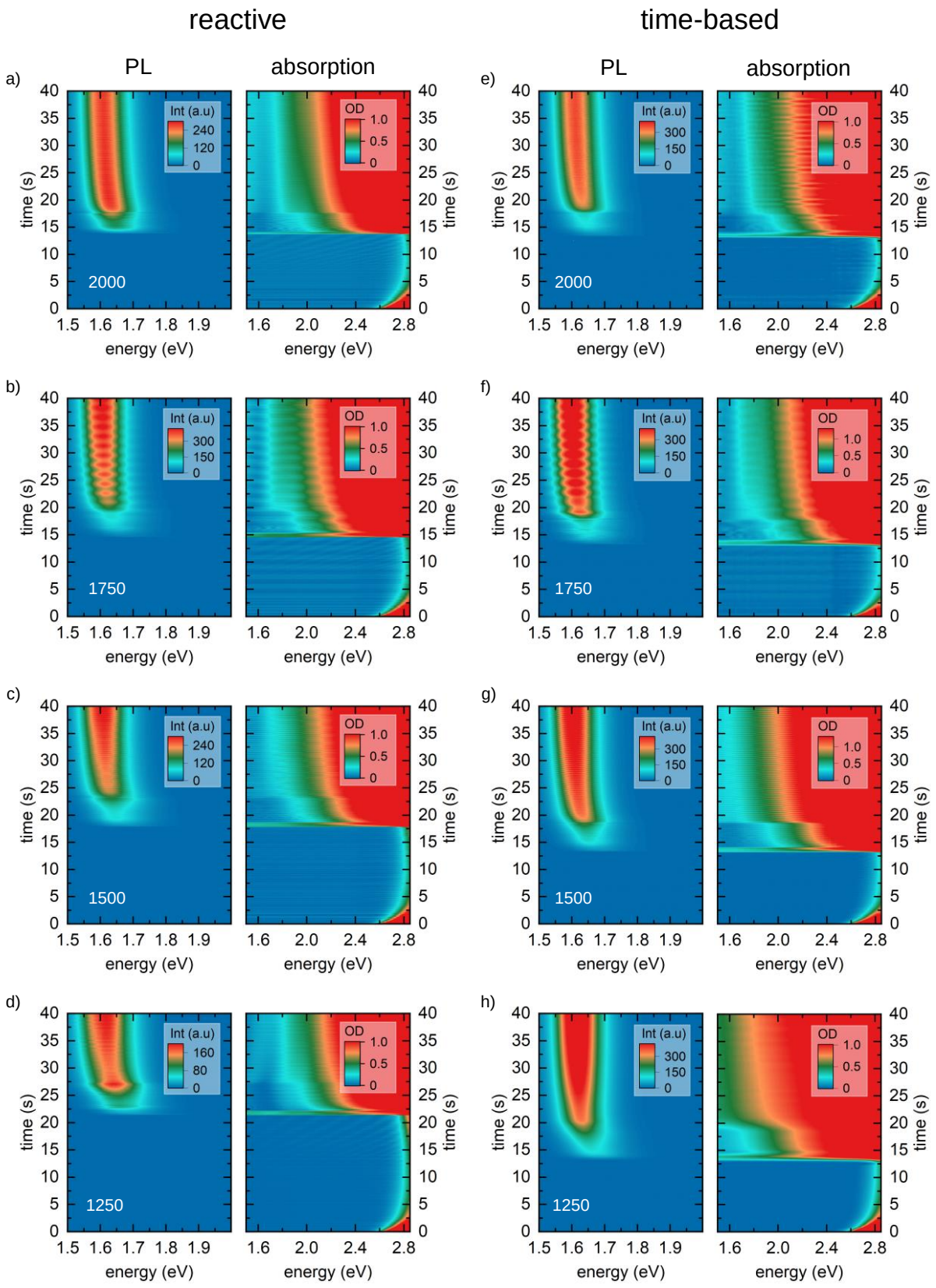

Figure S3: Heat maps of photoluminescence (PL), and absorption (OD) measurements of $MAPbI_3$ solutions during spin coating via the reactive spin coating approach (a-d) and for the time-based approach (e-h) for the different spin speeds (RPM in white numbers).

PL Peak Extraction and Crystallite size calculation

For fitting the PL spectra, we use an empirical line shape in the form of an asymmetric hyperbolic secant, that is

$$I(E) = I_0 \frac{2}{e^{\frac{E-E_0}{\sigma_1}} + e^{\frac{E-E_0}{\sigma_2}}} \quad \text{(S6)}$$

and extract the energy value of the maximum of this function for all recorded spectra over time.

This extracted peak position of the perovskite PL spectrum is considerably higher than typical bulk PL peak energies of 1.6 eV[3], which suggests the presence of a quantum confinement effect similar to a particle in a box approach. Considering this effect, the crystallite size *d* can be extracted from the energetic position of the PL peak via

$$E_{PL} = E_g + \frac{b}{d^2}\,, \quad \text{(S7)}$$

where we set the $MAPbI_3$ bulk band gap value E_g = 1.59 eV,[4–6] and the constant *b* = 3 eV nm^2,[7,8] based on literature values.

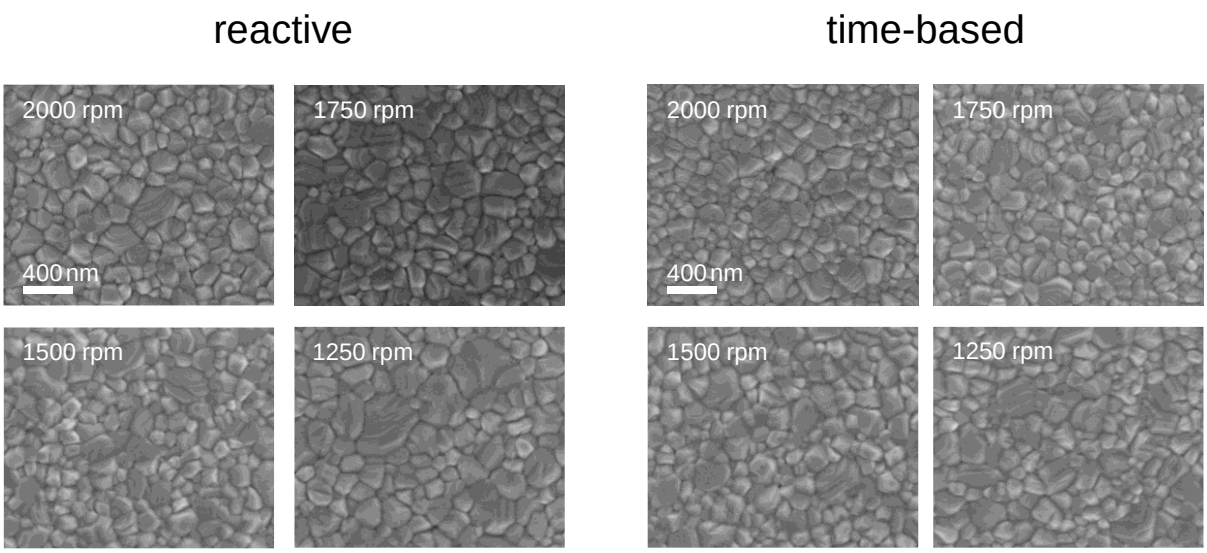

Figure S4: SEM top view images of the $MAPbI_3$ films fabricated via reactive (left) or time-based (right) spin coating approach at different spin speeds.

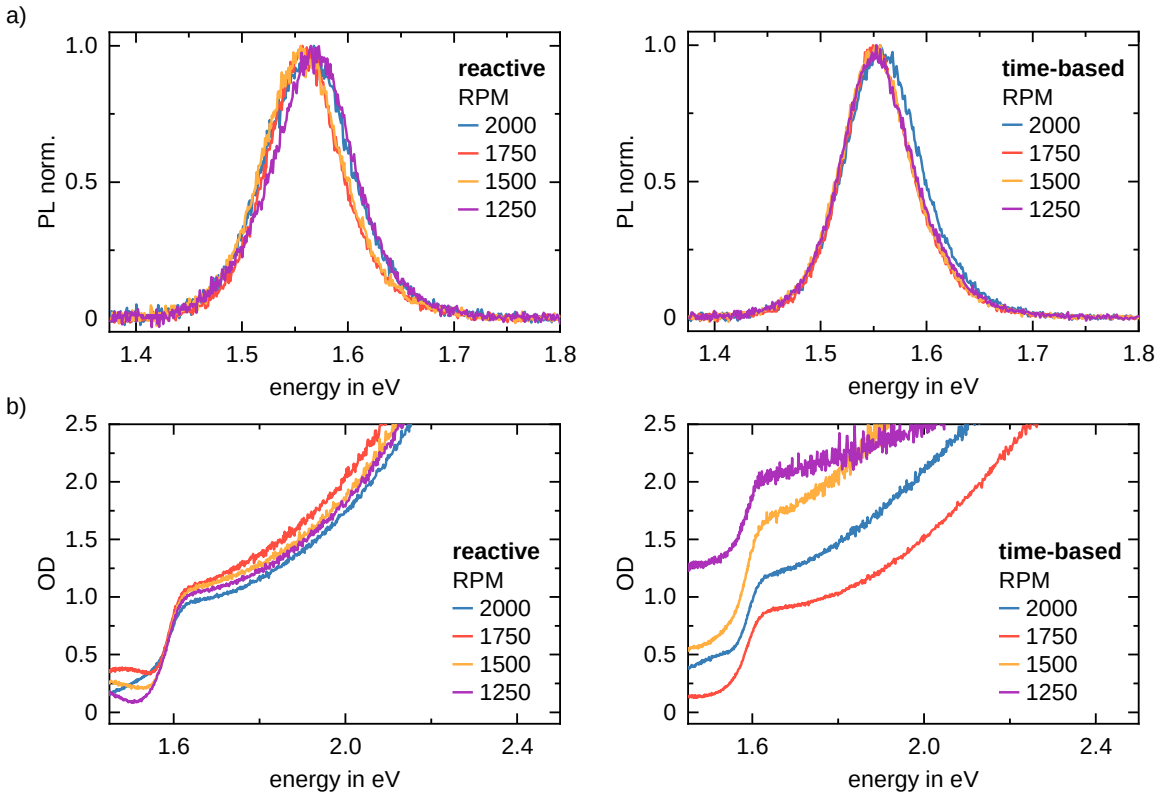

Figure S5: a) PL of $MAPbI_3$ films processed via reactive spin coating method (left) or via time-based spin coating (right) after annealing. The data is normalized to the maximum. b) OD spectra of $MAPbI_3$ films processed via reactive spin coating method (left) or via time-based spin coating (right) after annealing.

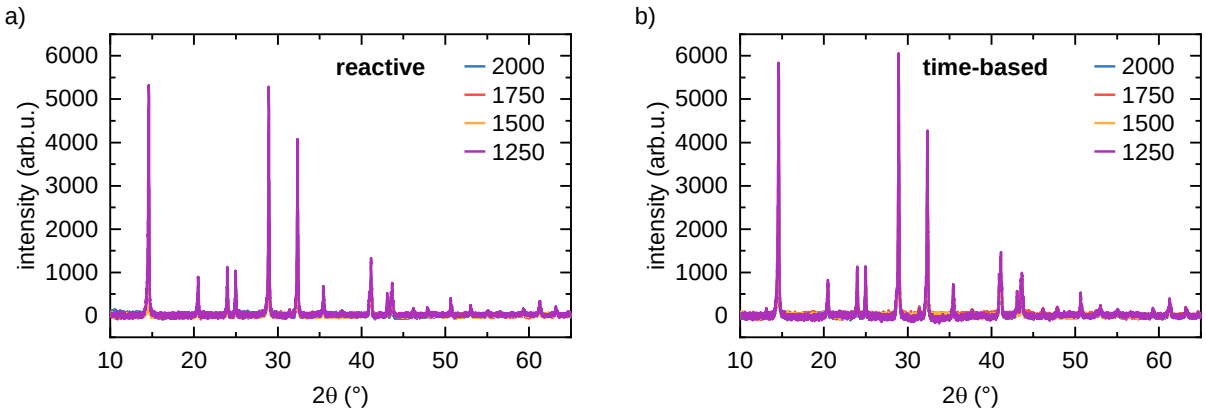

Figure S6: XRD patterns of the $MAPbI_3$ films fabricated via reactive (a) or time-based (b) spin coating approach at different spin speeds.

Section 3: $(MA_{0.13}FA_{0.83})Pb(I_{0.83}Br_{0.17})_3$

To investigate whether the reactive approach is also applicable to more complex mixed systems we also processed $(MA_{0.13}FA_{0.83})Pb(I_{0.83}Br_{0.17})_3$ (1.2M in DMF) via the reactive and time-based approach. We kept the value of the parameter of interest at 2000 nm and the antisolvent (AS) was dispensed once this value was reached for this solvent layer thickness. Analogously to the $MAPbI_3$ experiments, we also performed a set of coatings via the time-based approach where the AS was dispensed at a pre-set time. In the case of $(MA_{0.13}FA_{0.83})Pb(I_{0.83}Br_{0.17})_3$, this time was set to 11 s after spin coating start motivated by the fact that for a spin speed of 2000 RPM a solvent layer thickness of 2000 nm was reached after a spin coating time of 11 s.

Results and Discussion:

The heat maps for the different spin speeds and spin coating approaches are displayed in Figure S7. The behavior of the film formation is very similar to the discussed behavior for $MAPbI_3$ in the main text. As soon as the AS is dispensed the crystallization is induced and perovskite signatures (absorption edge and PL signal) are observed in the respective channels. Similar to the $MAPbI_3$ set, we tracked the PL peak position to extract the crystallite size as a function of time and to calculate the crystallite growth rate. By closer inspection of the PL data however, we noticed that our model to extract the crystallite size that assumes one species contributing to the PL signal is not fully applicable to the mixed composition. As it can be seen in Figure S8 there are at least two different emitting species (possibly iodine and bromine rich phases) present in the forming layer. The relative contribution of the signature at higher energies decreases with spin coating time. This can either be due to an improved halide mixing or a more efficient energy transfer from the high energy species to species at lower energies from which the emission then occurs.[9] Therefore, we only extracted the energetic position of the PL signal maximum (see Figure S9) for all spin speeds and the two processing approaches. However, to understand the film formation processes in detail, more investigations are needed, which will be focus of a follow-up investigation.

The final film properties (SEM images in Figure S10 and optical properties in Figure S11) of the processed films after annealing suggest a similar conclusion to the one that could be drawn for the $MAPbI_3$ experiments. The SEM images show that with

decreasing spin speed larger voids occur for the time-based approach. In contrast, for the reactive process, a similar perovskite layer is obtained independent of the spin speed. The optical characterizations reveal that – analogously to the $MAPbI_3$ results – the surface sensitive PL is identical for all films, proving that also in the case of $(MA_{0.13}FA_{0.83})Pb(I_{0.83}Br_{0.17})_3$ an identical top layer is formed for all films. In the OD spectra, agreeing with the $MAPbI_3$ findings, we observe a slight increase in scattering for the films processed via the time-based approach at lower spin speeds, which fits to the observed voids in the perovskite layer.

In conclusion, the results of the mixed composition $(MA_{0.13}FA_{0.83})Pb(I_{0.83}Br_{0.17})_3$ show good agreement with those of the $MAPbI_3$ experiments, discussed in the main text, demonstrating that the reactive spin coating approach is applicable for different perovskite compositions.

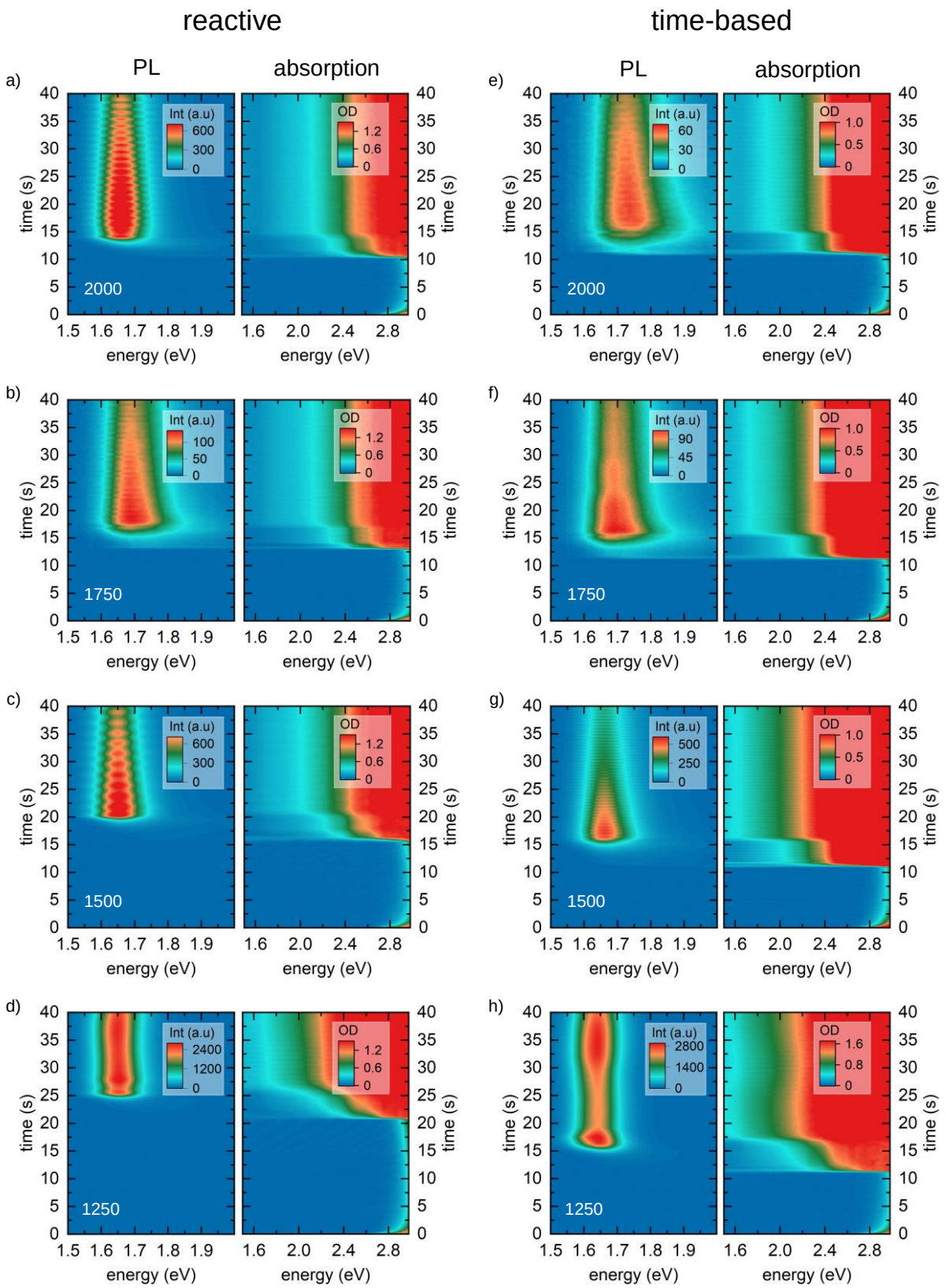

Figure S7: Heat maps of photoluminescence (PL), and absorption (OD) measurements of $(MA_{0.13}FA_{0.83})Pb(I_{0.83}Br_{0.17})_3$ solutions during spin coating via the reactive spin coating approach (a-d) and for the time-based approach (e-h) for the different spin speeds (RPM in white numbers).

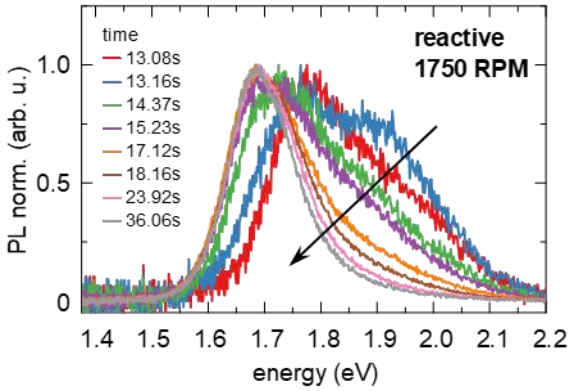

Figure S8: normalized PL spectra at different spin coating times for a $(MA_{0.13}FA_{0.83})Pb(I_{0.83}Br_{0.17})_3$ film processed at 1750 RPM. The arrow indicates decrease of an additional PL feature at higher energies with increasing spin coating time.

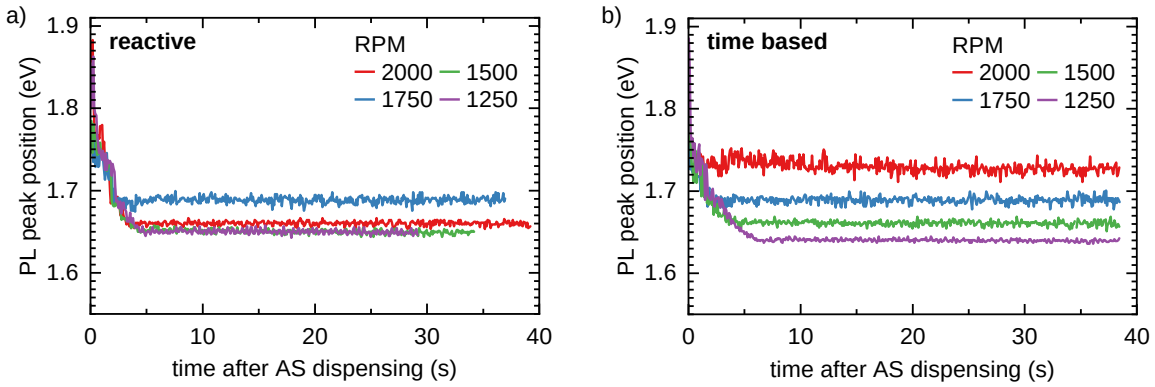

Figure S9: Time evolution of the energetic position of the maximum of the PL peak for $(MA_{0.13}FA_{0.83})Pb(I_{0.83}Br_{0.17})_3$ films processed via reactive (a) and time-based (b) spin coating for different RPMs.

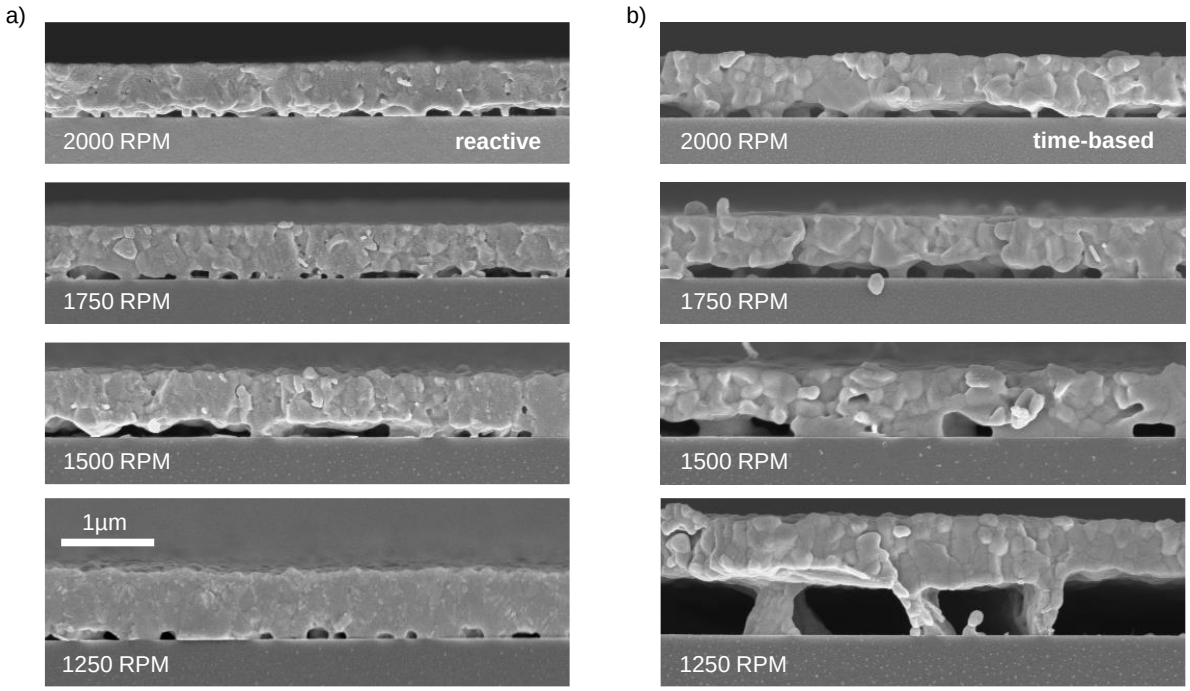

Figure S10: a) SEM cross-section images of the $(MA_{0.13}FA_{0.83})Pb(I_{0.83}Br_{0.17})_3$ films fabricated via reactive spin coating approach at different spin speeds. b) SEM cross-section images of the $(MA_{0.13}FA_{0.83})Pb(I_{0.83}Br_{0.17})_3$ films fabricated via time-based spin coating approach at different spin speeds.

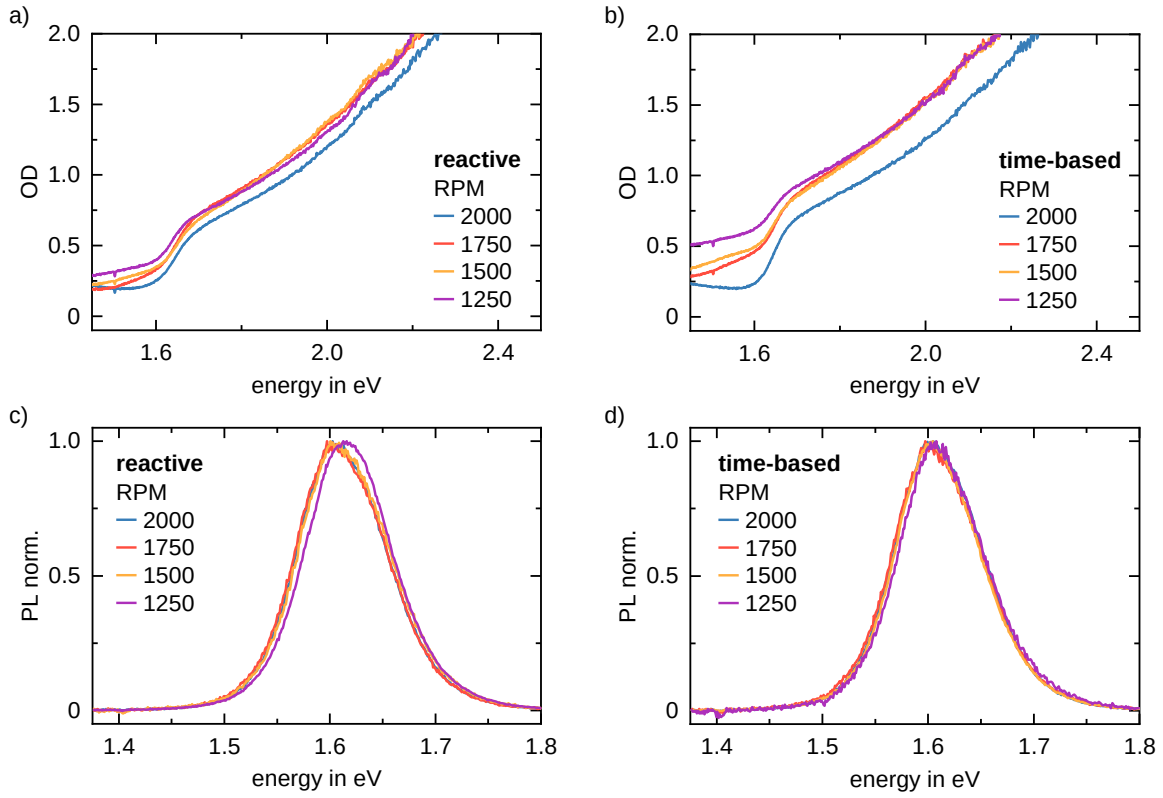

Figure S11: a) PL of $(MA_{0.13}FA_{0.83})Pb(I_{0.83}Br_{0.17})_3$ films processed via reactive spin coating method (left) or via time-based spin coating (right) after annealing. The data is normalized to the maximum. b) OD spectra of MAFA films processed via reactive spin coating method (left) or via time-based spin coating (right) after annealing.

Supporting References:

1) M. Buchhorn, S. Wedler and F. Panzer, *J. Phys. Chem. A*, 2018, **122**, 9115–9122.
2) S. Karpitschka, C. M. Weber and H. Riegler, *Chem. Eng. Sci.*, 2015, **129**, 243–248.
3) M. Chauhan, Y. Zhong, K. Schötz, B. Tripathi, A. Köhler, S. Huettner and F. Panzer, *J. Mater. Chem. A*, 2020, **8**, 5086–5094.
4) S. D. Stranks, P. K. Nayak, W. Zhang, T. Stergiopoulos and H. J. Snaith, *Angew. Chem. Int. Ed.*, 2015, **54**, 3240–3248.
5) T. Meier, T. P. Gujar, A. Schönleber, S. Olthof, K. Meerholz, S. van Smaalen, F. Panzer, M. Thelakkat and A. Köhler, *J. Mater. Chem. C*, 2018, **6**, 7512–7519.
6) Y. Kayanuma, *Phys. Rev. B*, 1988, **38**, 9797–9805.
7) K. P. Goetz, A. D. Taylor, F. Paulus and Y. Vaynzof, *Adv. Funct. Mater.*, 2020, **30**, 1910004.
8) A. Buin, R. Comin, A. H. Ip and E. H. Sargent, *J. Phys. Chem. C*, 2015, **119**, 13965–13971.
9) C. Greve, P. Ramming, M. Griesbach, N. Leupold, R. Moos, A. Köhler, E. M. Herzig, F. Panzer and H. Grüninger, *ACS Energy Lett.*, 2023, **8**, 5041–5049.